Reaction channel coupling effects for nucleons on ^{16}O: Induced undularity and proton-neutron potential differences

Journal Item

Reaction channel coupling effects for nucleons on ^{16}O: Induced undularity and proton-neutron potential differences

N. Keeley*
National Centre for Nuclear Research, ul Andrzeja Sołtana 7, 05-400 Otwock, Poland

R. S. Mackintosh†
School of Physical Sciences, The Open University, Milton Keynes, MK7 6AA, United Kingdom

(Received 13 November 2017; published 16 January 2018)

Background: Precise fitting of scattering observables suggests that the nucleon-nucleus interaction is l dependent. Such l dependence has been shown to be S-matrix equivalent to an undulatory l-independent potential. The undulations include radial regions where the imaginary term is emissive.
Purpose: To study the dynamical polarization potential (DPP) generated in proton-^{16}O and neutron-^{16}O interaction potentials by coupling to pickup channels. Undulatory features occurring in these DPPs can be compared with corresponding features of empirical optical model potentials (OMPs). Furthermore, the additional inclusion of coupling to vibrational states of the target will provide evidence for dynamically generated nonlocality.
Methods: The FRESCO code provides the elastic channel S-matrix S_{lj} for chosen channel couplings. Inversion, $S_{lj} \rightarrow V(r) + \mathbf{l}\cdot\mathbf{s}\,V_{\rm SO}(r)$, followed by subtraction of the bare potential, yields an l-independent and local representation of the DPP due to the chosen couplings.
Results: The DPPs have strongly undulatory features, including radial regions of emissivity. Certain features of empirical DPPs appear, e.g., the full inverted potential has emissive regions. The DPPs for different collective states are additive except near the nuclear center, whereas the collective and reaction channel DPPs are distinctly nonadditive over a considerable radial range, indicating dynamical nonlocality. Substantial differences between the DPPs due to pickup coupling for protons and neutrons occur; these imply a greater difference between proton and neutron OMPs than the standard phenomenological prescription.
Conclusions: The onus is on those who object to undularity in the local and l-independent representation of nucleon elastic scattering to show why such undulations do not occur. This work suggests that it is not legitimate to halt model-independent fits to high-quality data at the appearance of undularity.

DOI: 10.1103/PhysRevC.97.014605

I. INTRODUCTION

The substantial contribution of reaction channel coupling to essentially all direct nuclear reactions is well established. Modern coupled reaction channel (CRC) calculations, with full finite range transfer and nonorthogonality corrections, have contributed to our understanding of a wide variety of direct reactions. Their application to light-ion scattering, to nucleon scattering in particular, reveals contributions to the elastic-scattering potential that extend to the nuclear center. The nucleon optical model potential (OMP) is of particular interest since its negative-energy extension is fundamental to the shell model, but there are still basic features of it which are more uncertain than commonly acknowledged [1]. In the present work we apply established methods to examine the contribution of reaction channels to the interaction potential for nucleons scattering from ^{16}O. For protons scattering from ^{16}O exceptional data are available (see, e.g., Refs. [2,3]) which cannot be fit with standard parameterized potentials. Although there are insufficient good data for neutron elastic scattering from ^{16}O to evaluate calculated properties in a meaningful way, we present differences between derived proton and neutron potentials that arise from differences in transfer Q values and related properties.

Previous CRC calculations, presented in Ref. [4], showed that coupling between the elastic channel and pickup (deuteron) channels makes a substantial contribution to the OMP for protons scattering from ^{40}Ca. Furthermore, the contribution to proton potentials arising from the inelastic coupling to vibrational nuclear states was presented in Ref. [5]. Here, we present calculations of both kinds of coupling for proton and neutron scattering from ^{16}O with the following objectives:

(i) Test the generality of channel-coupling contributions to OMPs, and the dependence of such contributions upon the nature of the coupling and other parameters.
(ii) Explore links between channel coupling and phenomenology. Nucleon elastic scattering from ^{16}O has proven to be hard to fit with smooth phenomenological potentials; there are indications that explicitly l-dependent potentials are required [6,7]. Moreover it is known that l-independent potentials having the same elastic-scattering S matrix as l-dependent potentials exhibit undulatory (wavy) features that include local

*nicholas.keeley@ncbj.gov.pl
†raymond.mackintosh@open.ac.uk

emissive regions in the surface and elsewhere. There are also indications of undulatory features from precise model-independent fitting. We therefore explore the propensity for coupling between the elastic channel and reaction and inelastic channels to generate dynamic polarization potentials (DPPs) that have undulatory features, including regions of emissivity. Here, as elsewhere, references to DPPs should be understood to refer to local and l-independent representations of the formal DPPs defined by Satchler [8], based on the formalism of Feshbach [9,10].

(iii) By comparing DPPs for proton and neutron elastic scattering generated by coupling to pickup (and other) channels, identify sources of differences between proton and neutron optical potentials for $T = 0$ nuclei. In particular, such differences can be expected to exceed the well-known term due to Perey [11]: $V_p - V_n = 0.4Z/A^{1/3}$, where V by convention is positive for an attractive potential. This Perey term implies that the proton-^{16}O OMP should be 1.27 MeV deeper than the neutron-^{16}O OMP, but there is scope for larger effects due to the significant differences between proton and neutron pickup on ^{16}O. For example, the (p,d) and (n,d) Q values differ substantially.

In this work, we determine a local representation of the DPP, which arises from specific channel couplings, in the following way: The elastic channel S-matrix S_{lj} from a coupled reaction channel (CRC) calculation [4], or coupled channel (CC) calculation [5], is in each case subjected to $S_{lj} \rightarrow V(r) + \mathbf{l}\cdot\mathbf{s}\, V_{SO}(r)$ inversion, where $V(r)$ and $V_{SO}(r)$ are l independent. The "bare" potential, i.e., the elastic channel potential of the appropriate CC or CRC calculation, is subtracted at each radial point from the inverted potential derived from the elastic channel S matrix. This procedure yields a local and l-independent representation of the intrinsically nonlocal and l-dependent [8–10,12] DPP generated by the specific channel coupling. It can therefore be regarded as the contribution made by the relevant coupled channels to the local OMP.

The procedure just described, involving coupled-channel calculations followed by S-matrix inversion, has been applied many times, and an account of it can be found in Ref. [13]. A discussion of the dynamic nonlocality of the DPPs calculated in this way and a comparison of alternative inversion methods can be found in Ref. [14]. The results of two recent applications of CC-plus-inversion are relevant to the present work, with results that will be mentioned below. They both relate to elastic scattering of nucleons on ^{40}Ca: Ref. [4] presents DPPs due to coupling to pickup channels and Ref. [5] presents DPPs for coupling to vibrational states. The present work, concerning nucleon scattering on ^{16}O, involves both kinds of coupling and identifies properties of the combined DPPs which relate to the induced dynamical nonlocality. The present work also reveals some significant differences between the reaction channel DPPs for protons and neutrons on ^{16}O.

A characteristic property of DPPs found by the coupled-channel-plus-inversion method is the occurrence of undulatory features, including radial regions where the imaginary term is emissive. This applies for heavy-ion scattering (see, e.g., Refs. [15,16]) and nucleon scattering on ^{40}Ca [14]. In this work we verify that such undularities are also present, for both neutron and proton scattering, in the DPP for the lighter, surface-dominated ^{16}O nucleus. Furthermore, it is important to substantiate the appearance of undulatory and emissive features in DPPs as a general property, not least because of the relationship [17] between undulatory properties and the l dependence of the OMP. While the similarities between the resulting DPPs for protons and neutrons will support the general properties of the DPPs that we find, the differences will also be of interest.

As mentioned, there are data for proton scattering on ^{16}O that are both precise and of wide angular range. We have not attempted to adjust the proton potential to fit these data with our most elaborate CRC calculation. Instead we have chosen the more modest goal of showing that certain characteristics of nucleon potentials, undularity and emissive regions for example, are generated by channel coupling. By keeping the bare potential fixed, we are able to study the variety of effects induced by reaction channels and inelastic channels and explore the interactions of these effects, leading to information on coupling-induced nonlocality.

In Sec. II we give details of the reaction coupling calculations, define quantities relating to the inversion calculations, and provide a labeled list of cases studied. In Sec. III the calculations involving inelastic coupling are presented. Section IV presents the pickup coupling calculations. Section V identifies evidence for dynamically generated nonlocality. Section VI discusses inversion uncertainties and their bearing upon deduced undularity. Section VII summarizes the results and relates them to past and possible future work.

II. SPECIFICATION OF THE CALCULATIONS

We study the distinctive contributions to the nucleon OMP of coupling to (i) inelastic channels and (ii) reaction (pickup) channels. We also study their combined effects. Examination of the combined effects of collective coupling and reaction coupling makes it possible to evaluate the extent to which particular contributions to the local DPP add, since as discussed elsewhere [13,18], this provides evidence for dynamically generated nonlocality. Dynamical nonlocality is not directly evident in the inverted local potential that results from a single coupling.

There is an obvious but important difference between the vibrational and pickup calculations. The excitation energies of the vibrational states of ^{16}O are the same for protons and neutrons, but there are important differences in the pickup couplings. The Q-values for pickup leading to ^{15}O and ^{15}N are significantly different, -13.44 MeV and -9.90 MeV, respectively. The transfer form factors and momentum-matching characteristics also differ significantly. The consequent difference between the DPPs for (p,d) and (n,d) will contribute to the difference in the proton and neutron OMPs for this $T = 0$ target nucleus.

A. The coupled channel and coupled reaction channel calculations

The CC and CRC calculations were performed by using the code FRESCO [19]. The parameters of the bare, no-coupling,

optical potentials in the entrance channels were taken from Table 1 of Ref. [6] for both protons and neutrons. The parameters chosen constitute the l-independent part of the best-fit l-dependent potential for the $p + {}^{16}$O elastic-scattering data at an incident energy of 30.1 MeV. Couplings to the 6.13 MeV 3^- state and a 2^+ state at an excitation energy of 22 MeV were included in the calculations except where otherwise stated. The $B(E3; 0^+ \rightarrow 3^-)$ value was taken from Table VII of Ref. [20] and the corresponding nuclear deformation length, $\delta_3 = 1.71$ fm, from Ref. [21]. We followed Pignanelli *et al.* [22] in placing a 2^+ state at an excitation energy of 22 MeV to represent the giant quadrupole resonance (GQR). The coupling strength was arbitrarily fixed at 80% of the energy-weighted sum-rule limit given in Ref. [22]. In this respect we did not attempt to model accurately the excitation of the GQR in ^{16}O, merely to investigate the possible influence of such a coupling on the DPP in light of the significant effect on the elastic-scattering angular distribution at backward angles found by Pignanelli *et al.* [22].

The ^{16}O$(p,d)^{15}$O and ^{16}O$(n,d)^{15}$N pickup couplings were both included by using prior form finite-range CRC including full complex remnant terms and nonorthogonality corrections. The exit channel deuteron optical potential parameters were identical in both cases in the interest of keeping both sets of calculations as similar as possible, and were the 16.3 MeV $d + {}^{16}$O set from the compilation of Perey and Perey [23]. The $\langle d \mid p + n \rangle$ overlaps were calculated by using the Reid soft-core potential [24]. Pickup to the 0.0 MeV $1/2^-$ and 6.18 MeV $3/2^-$ states of ^{15}O and the 0.0 MeV $1/2^-$ and 6.32 MeV $3/2^-$ states of ^{15}N was included in the (p,d) and (n,d) calculations, respectively. The transferred neutron and proton were bound to their respective ^{15}O and ^{15}N cores in Woods–Saxon wells with parameters taken from Ref. [25].

B. Inversion calculations

A key part of our method involves $S_{lj} \rightarrow V(r) + \mathbf{l} \cdot \mathbf{s}\, V_{\rm SO}(r)$ inversion, and some of the related terminology will be referred to in what follows. The S matrices are inverted by using the iterative-perturbative (IP) $S_{lj} \rightarrow V(r) + \mathbf{l} \cdot \mathbf{s}\, V_{\rm SO}(r)$ inversion algorithm presented in Refs. [26–29]. The IP inversion is implemented in the code IMAGO [30] which quantifies the difference between the S^t_{lj} to be inverted and the S^i_{lj} of the inverted potential in terms of the S-matrix distance σ defined as

$$\sigma^2 = \sum_{lj} \left| S^t_{lj} - S^i_{lj} \right|^2. \tag{1}$$

The iterations of the IP method start from a "starting reference potential" (SRP), which in all cases presented here was the bare potential of the CC or CRC calculation. In some cases the SRP is included in plots of the inverted potential, so that the contribution of the channel coupling to the inverted l-independent potential is apparent as the difference between the SRP and the inverted potential. It has long been established that the IP method can yield inverted potentials that are effectively independent of the SRP and the uniqueness of the inverted potential can be tested by the use of alternative "inversion bases," see Refs. [28,29]. For most of the present results a Gaussian inversion basis was used, but some results with a Bessel-function inversion basis will also be presented.

The tendency for increasing undularity to appear in solutions as σ becomes very small will be addressed in Sec. VI in relation to the significance of the potential undulations.

C. List of cases studied

In the tables, text, and figure captions, we refer to specific calculations with labels "CC2" etc., as follows:

CC2:	coupling of the proton elastic channel to the 22 MeV 2^+ GQR of ^{16}O.
CC3:	coupling of the proton elastic channel to the 6.13 MeV 3^- state of ^{16}O.
CC23:	coupling of the proton elastic channel to both the 2^+ and 3^- states.
CC23noCouex:	like CC23 but with Coulomb excitation omitted.
CC23n:	coupling of the neutron elastic channel to both the 2^+ and 3^- states.
CRC:	coupling of the proton elastic channel to both the $\frac{1}{2}^-$ and the $\frac{3}{2}^-$ states of ^{15}O plus the CC23 collective states.
CRCn:	coupling of the neutron elastic channel to both the $\frac{1}{2}^-$ and the $\frac{3}{2}^-$ states of ^{15}N plus the CC23n collective states.
CRC-noInel:	coupling to the $\frac{1}{2}^-$ and $\frac{3}{2}^-$ states of ^{15}O *only*.
CRCn-noInel:	like CRC-noInel but for neutron scattering, and coupling to states of ^{15}N.
CRC-noinelwxp5:	like the CRC-noInel case but with the depth of the imaginary potential in the pickup channel multiplied by 0.5.

Note that, as indicated in the above list, "CRC" as a designation of a particular case studied has a specific meaning that differs from its earlier general reference to a coupled reaction channel calculation.

D. Evaluating results of calculations

We refer to the elastic channel potential of the CC or CRC calculation as the bare potential and each component of the DPP (real central, imaginary central, real spin orbit, imaginary spin orbit) is the corresponding component of the inverted potential when the relevant component of the bare potential has been subtracted. Note that the DPP will always have an imaginary spin-orbit term irrespective of whether the bare potential has such a component. Note also that the S matrix from the CC or CRC calculation will always satisfy the unitarity limit $|S_{lj}| \leqslant 1$ even when the inverted imaginary potential has particular radial ranges where it is emissive, i.e., it has the wrong sign for absorption.

In many cases the radial dependence of the DPPs will be presented graphically, but the DPPs will also be quantified in terms of the volume integrals per target nucleon, so that $\Delta J_{\rm R}$ is the difference between the volume integral (standard normalization [8]) of the real central term of the inverted potential and the corresponding term for the bare potential.

TABLE I. The volume integrals of the DPPs for the cases identified in the first column, derived by using a Gaussian inversion basis, in MeV fm^3. Also given are the corresponding quantities ΔCS, σ(inel) both in mb, and their ratio obtained directly from the CC or CRC calculation.

Case	ΔJ_R	ΔJ_I	ΔJ_{SOR}	ΔJ_{SOI}	ΔCS	ΔCS/ΔJ_I	σ(inel)	ΔCS/σ(inel)
CC2	2.51	15.73	−1.562	1.124	31.21	1.98	16.10	1.94
CC3	4.46	18.65	−0.144	0.634	51.34	2.75	53.29	0.96
CC2+CC3	6.97	34.38	−1.706	1.808	82.55	(2.40)	69.39	(1.19)
CC23	5.81	34.55	−1.852	2.101	73.60	2.13	63.02	1.17
CC23noCouex	5.44	36.43	−1.969	2.360	76.26	2.09	64.92	1.13
CC23n	8.19	30.65	−1.439	−0.197	76.16	2.48	70.38	1.08
CRC	61.07	134.56	−11.811	6.200	229.49	1.705	73.34	3.13
CRCn	0.45	106.60	−7.434	−0.336	229.53	2.15	95.45	2.405
CRC-noInel	39.30	87.71	−12.72	3.75	212.91	2.43	31.04	6.86
CRCn-noInel	7.70	90.11	−7.51	−4.945	196.44	2.18	52.28	3.76
CRC-noInel+CC23	45.11	122.26	−14.57	5.851	286.51	(2.34)	94.06	(3.04)
CRCn-noInel+CC23n	15.89	120.76	−8.949	−5.142	272.6	(2.26)	122.66	(2.22)
CRC-noinelwxp5	23.82	99.13	−30.22	13.38	218.68	2.19	68.44	3.20

The other three terms are denoted ΔJ_I, ΔJ_{SOR}, and ΔJ_{SOI}, with all values in MeV fm^3. These quantities are presented in Table I, which will be referred to throughout this work.

The values of ΔJ_R result from subtracting two relatively large numbers. The volume integrals of potentials that are undulatory in the surface may not closely reflect the magnitude of the coupling effect. As a result, we find some variance in ΔJ_R even in cases where the overall shape of the real central potential appears to be very well determined.

We explain some points about Table I:

(i) The lines with a plus sign in column 1 (e.g., CC2 + CC3) present values that are the numerical sums of the indicated quantities for, e.g., CC2 and CC3.
(ii) ΔCS is the change in reaction cross section arising from the coupling as calculated directly from the elastic-scattering S-matrix S_{lj}.
(iii) σ(inel) is the cross section for populating the inelastic channels (CC cases), reaction channels plus inelastic channels (CRC cases), and reaction channels alone in the CRC-noinel cases.

Figure 1 presents the differential cross section and analyzing power for protons for the cases without coupling (bare potential) and the cases with coupling, labeled CC2, CC23, and CRC. The bare potential is the same in all calculations. From this figure it is evident that pickup coupling has a large effect on the analyzing power, predicting a large contribution of this coupling to the spin-orbit potential. Clearly, the angular distribution for the CRC case does not fit the data, represented by the large dots. Searching on all the relevant parameters for a perfect fit for combined CC and CRC calculations was not attempted. Although Ref. [4], relating to pickup coupling for ^{40}Ca, presented "linearity tests" which suggested that the DPPs are not strongly dependent upon the choice of bare potential, those tests involved better fits than those in Fig. 1. However, the general qualitative features presented here are well determined.

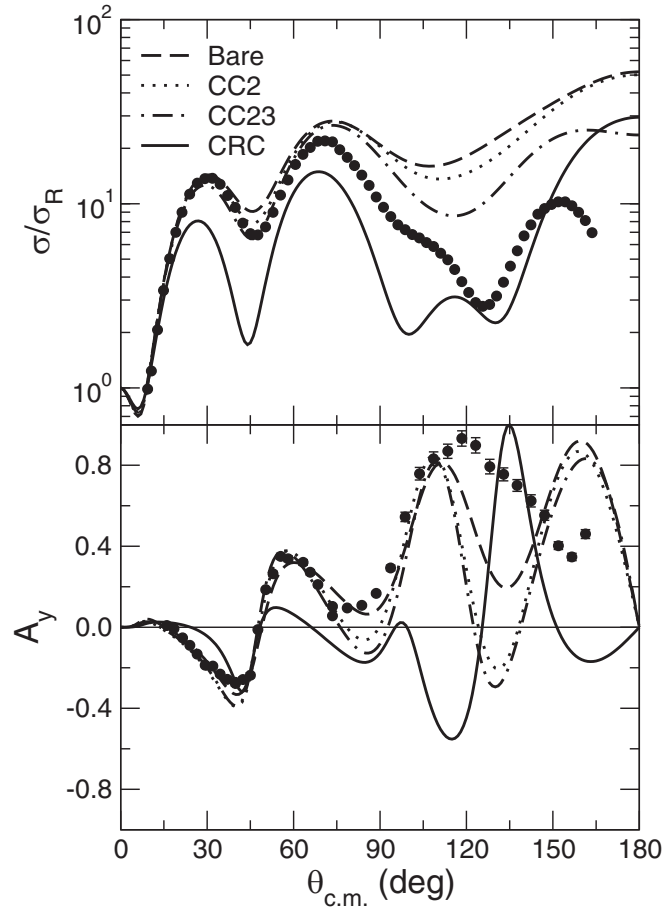

FIG. 1. For 30.1 MeV protons on ^{16}O, the effects on the differential cross section (upper panel) and analyzing power (lower panel) of coupling successively more channels to the elastic channel. The dashed line (Bare) is for no coupling, the dotted line shows the effect of coupling to the 2^+ state (GQR), the dash-dotted line is with coupling to the 3^- state added, and the solid line is with the full pickup coupling added. The large dots represent the experimental measurements [2,3].

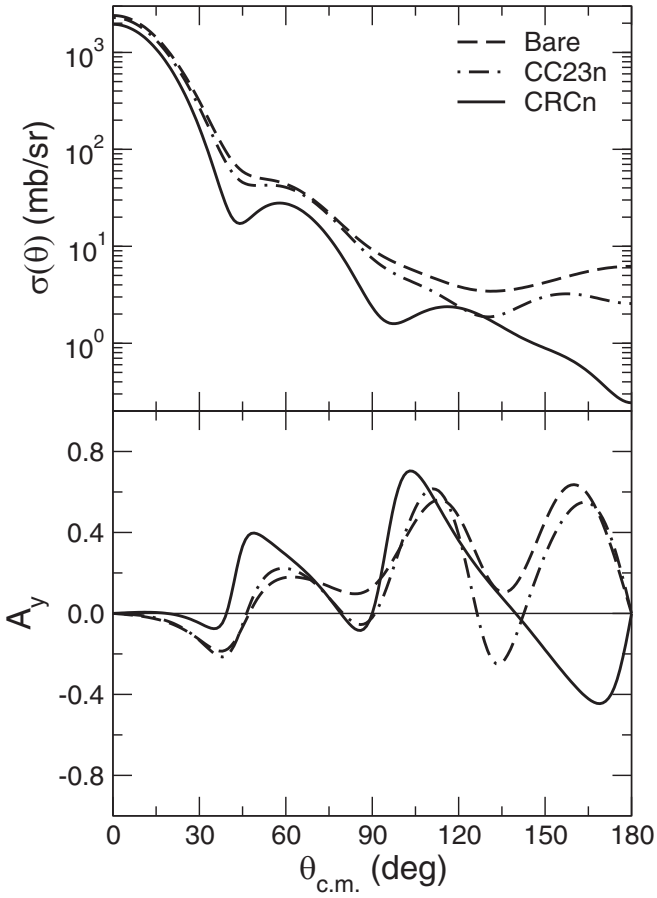

FIG. 2. For 30.1 MeV neutrons on ^{16}O, the effects of coupling successively more channels to the elastic channel on the differential cross section (upper panel) and analyzing power (lower panel). The dashed line (Bare) is for no coupling, the dot-dashed line shows the effect of coupling to the 2^+ and 3^- states, and the solid line is with the full pickup coupling added to the collective states. (No experimental measurements are available.)

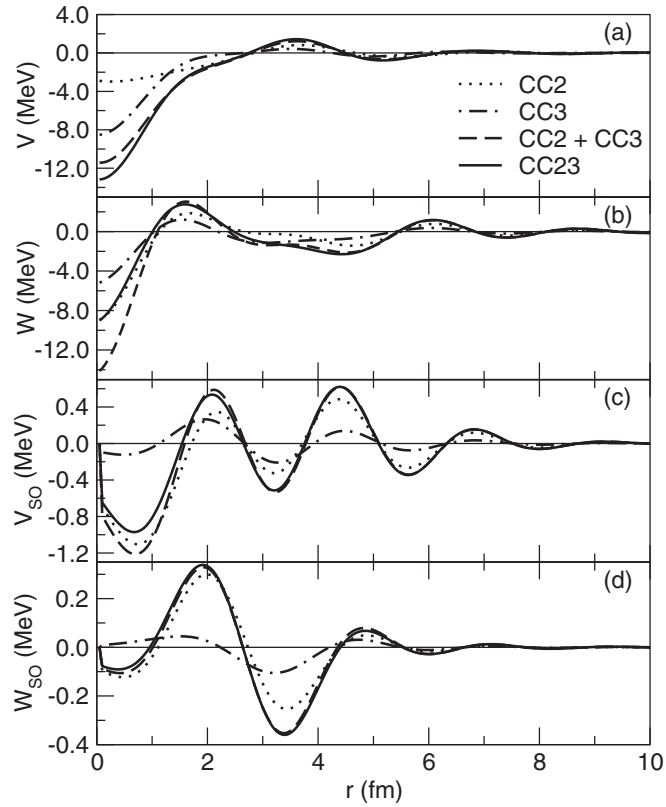

FIG. 3. For 30.1 MeV protons on ^{16}O, the DPPs arising from coupling to the 2^+ and 3^- vibrational states of ^{16}O. The dotted line (CC2) is for coupling to the 2^+ state, the dash-dotted line (CC3) is for coupling to the 3^- state, the dashed line presents the numerical sum of the CC2 and CC3 DPPs, and the solid line is the DPP for the CC23 case in which both vibrational states are coupled to the elastic channel. Panels (a)–(d) present the real central, imaginary central, real spin-orbit, and imaginary spin-orbit terms, respectively.

We note that on both theoretical [31] and empirical [32] grounds, the proton-^{16}O interaction has a parity dependence arising from exchange terms that are not of the knock-on type; these are omitted in the present calculations.

Figure 2 presents the differential cross section and analyzing power for neutrons for the cases without coupling (bare potential) and the cases with couplings labeled CC23n and CRCn. There are no experimental data for this case. At the most backward angle, the neutron elastic-scattering differential cross section is reduced by the collective coupling by a factor of about 2.4, and when pickup coupling is included, reduced by a factor of about 24.

III. INELASTIC COUPLING CONTRIBUTIONS TO NUCLEON OPTICAL MODEL POTENTIAL FOR ^{16}O

A. Dynamic polarization potentials for proton scattering

Figure 3 presents the DPPs arising from the coupling to the vibrational states for protons scattering from ^{16}O. The DPPs for coupling to the 2^+ (CC2 case) and 3^- (CC3 case) states are both shown, together with their numerical sum. This sum can be compared with the DPP for the CC23 case in which both states are coupled. This comparison is relevant to the question of the dynamical nonlocality generated by channel coupling, as discussed below. Note that, as in all similar figures to follow, the vertical scale of the potentials has been adjusted appropriately and is different for each component.

The following particular features are revealed in Fig. 3:

(i) All the DPPs are undulatory, and all the radial shapes have the same general features.

(ii) The imaginary central terms all have emissive regions. Not apparent in Fig. 3 is the fact that, in the CC2 and CC23 cases, the emissive region around 6 fm is such as to make the total inverted potential definitely emissive at that point.

(iii) Although the CC2 central DPP is mostly smaller in magnitude than the CC3 central DPP, CC2 coupling evidently makes the dominant contribution to the real and imaginary spin-orbit terms. This feature is reflected in the volume integrals presented in Table I and might be related to the large momentum transfer in the excitation of the 2^+ state.

(iv) The sum of the CC2 and CC3 DPPs is quite close to the CC23 DPP except for significant differences near the nuclear center. In fact the sum of the CC2 and CC3 spin-orbit DPPs is hard to distinguish from the CC23 DPP beyond about 3 fm.

(v) Although channel coupling generates quite significant attraction near the nuclear center ($r \leqslant 1$ fm), the repulsive region around 4 fm (the surface region of the bare potential real term) results in a numerically very small overall contribution to $\Delta J_{\rm R}$. This quantity is therefore an imperfect single quantifier of the effect of coupling on the real central term of the potential.

The magnitudes of $\Delta J_{\rm R}$ and $\Delta J_{\rm I}$ for CC2 are somewhat smaller than for CC3. This is in contrast with the inelastic cross sections σ(inel) in Table I, quantities not derived from the inversion but directly from the CC calculations. For the excitation of the 3^- state, σ(inel) is 53.29 mb, a factor of 3.3 greater than σ(inel) for the 2^+ state. Interestingly, the increase in reaction cross section for CC3, 51.34 mb, is just 1.6 times greater than for CC2 and is also less than the corresponding σ(inel). This indicates that 3^- inelastic scattering reduces absorption from all other processes, while the opposite is the case for 2^+ coupling.

The strongly undulatory nature of the inverted potentials (for the imaginary spin-orbit component, the DPP is the inverted potential) may not be expected on the basis of the apparent phenomenological success of smooth potentials. Yet, the manner in which the quite different CC2 and CC3 results for the imaginary spin-orbit component in Fig. 3 add so closely to the CC23 result arguably confirms that the undulations are not artifacts of the $S_{lj} \rightarrow V(r) + \mathbf{l}\cdot\mathbf{s}\, V_{\rm SO}(r)$ inversion process.

B. The nucleon optical model potential: Comparing proton and neutron dynamic polarization potentials

Figure 4 compares the DPPs for protons (solid lines) and neutrons (dot-dashed lines) generated by coupling to both the 2^+ and 3^- states (cases CC23 and CC23n). The central terms are very similar, including the existence of emissive features around 1.5 and 6 fm in the imaginary central term. The latter leads to emissivity around 6 fm in the full imaginary potential. There are some differences between the central terms and these are greatest at smaller radii, but the general features of the central terms of the DPPs are the same for protons and neutrons.

By contrast, the neutron spin-orbit terms appear quite different from those for protons. However, the spin-orbit DPPs are small in magnitude, and the actual numerical differences between the proton and neutron spin-orbit DPPs are not greater than the differences between the proton and neutron central DPPs.

Figure 4 also presents, as dashed lines barely distinguishable from the solid lines, the DPP for the proton case with the Coulomb excitation switched off (case CC23noCouex). This shows clearly that the differences between the proton and neutron DPPs are not a consequence of the Coulomb excitation in the proton case.

We see from Table I that, in all cases, the effect of inelastic channel coupling is an overall reduction, as measured by $\Delta J_{\rm SOR}$, in the real spin-orbit potential.

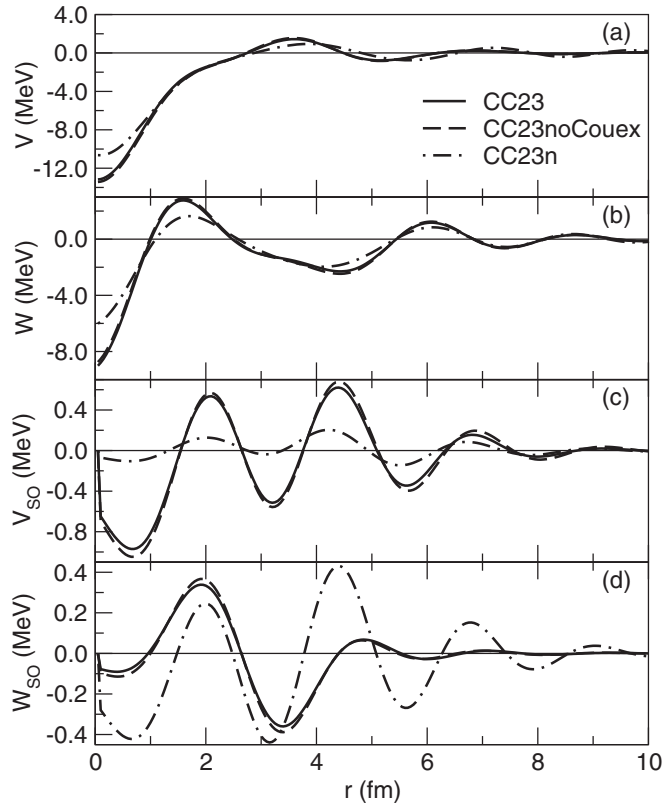

FIG. 4. For 30.1 MeV protons and neutrons on ^{16}O, the DPPs arising from coupling to both the 2^+ and 3^- vibrational states of ^{16}O. The solid lines present the CC23 DPP shown in Fig. 3, the dashed lines present the DPP for the same case in which the Coulomb excitation is turned off, and the dot-dashed lines show the DPP for neutron scattering with coupling to the same pair of vibrational states. Panels (a)–(d) present the real central, imaginary central, real spin-orbit, and imaginary spin-orbit terms, respectively.

IV. PICKUP COUPLING CONTRIBUTIONS TO NUCLEON OPTICAL MODEL POTENTIAL FOR ^{16}O

A. Dynamic polarization potential for protons, coupled reaction channel coupling

The dotted lines in Fig. 5 present the bare potential that was employed in all calculations in this work. In that figure, the bare potential is compared with two inverted potentials for the CRC case, i.e., which here signifies both pickup coupling leading to states of ^{15}O and coupling to the two collective states of ^{16}O. The dashed lines, labeled pot3, present the outcome of the penultimate stage of the iterative inversion process. Pot4, represented by the solid lines, was the final stage at which the fit to arg S_{lj} and $|S_{lj}|$ for all partial waves up to $l = 15$ was effectively perfect. For pot3, the inversion S matrix distance $\sigma = 3.3 \times 10^{-4}$ represents a near perfect fit to S_{lj} up to about $l = 10$, while the fit up to $l = 15$, pot4, corresponds to $\sigma = 2.4 \times 10^{-5}$. The improved fit to S_{lj} between $l = 10$ and $l = 15$ corresponds to the difference between pot3 and pot4. We have taken pot4 to be the inverted potential in Table I and elsewhere, but we note that pot3 and pot4 fit the elastic-scattering observables calculated by the reaction channel calculation equally

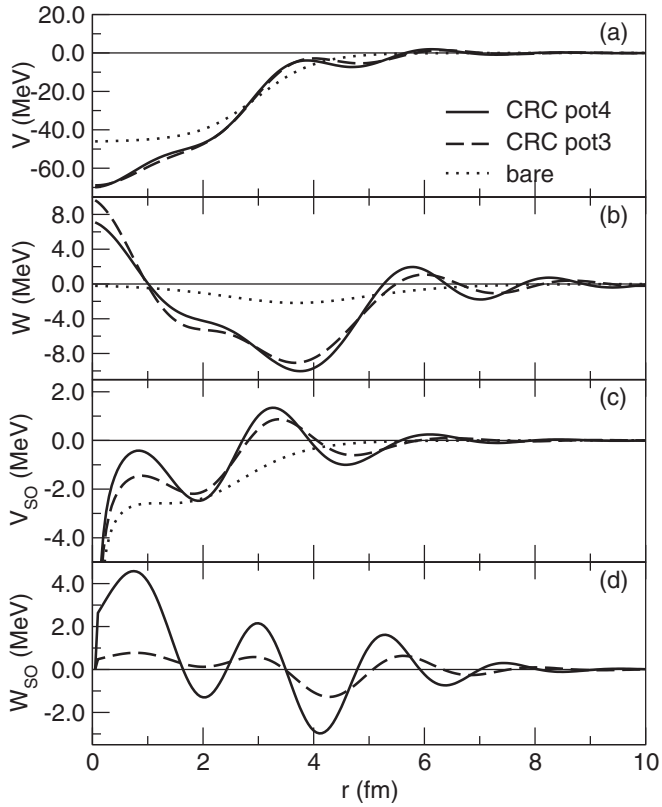

FIG. 5. For 30.1 MeV protons on ^{16}O, inverted potentials, labeled pot3 (dashed) and pot4 (solid), for the CRC case together with the bare potential; dotted lines. Pot3 and pot4 are successive solutions to IP inversion, as explained in the text. The CRC cases include coupling to two pickup states together with the two vibrational states. Panels (a)–(d) present the real central, imaginary central, real spin-orbit, and imaginary spin-orbit terms, respectively.

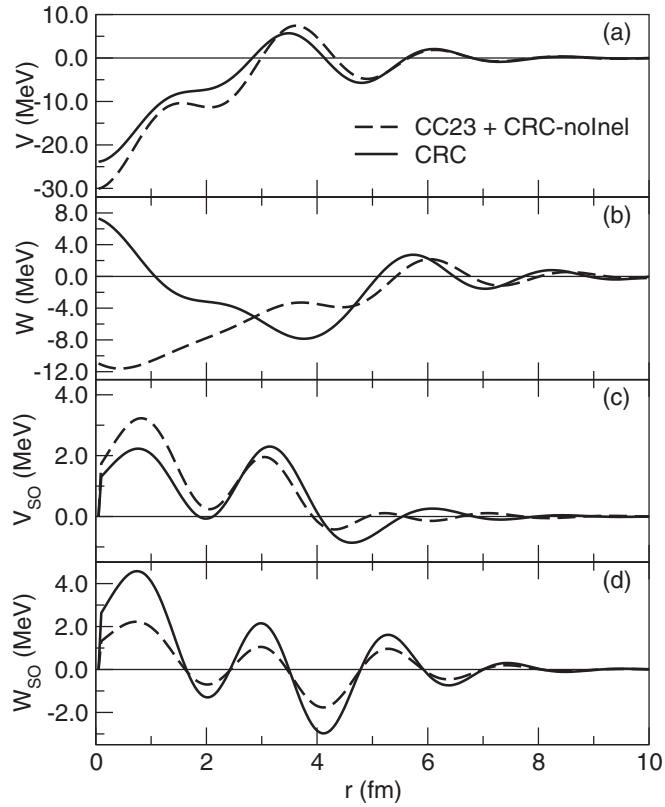

FIG. 6. For 30.1 MeV protons on ^{16}O, the DPP pot4 for the CRC calculation, solid lines, together with the numerical sum of the DPP for CRC-noInel and the CC23 DPP, dashed lines. Panels (a)–(d) present the real central, imaginary central, real spin-orbit, and imaginary spin-orbit terms, respectively.

well (indistinguishable graphically). In Sec. VI we discuss the significance of changes in a potential that improve the fit to S_{lj} without making experimentally detectable changes to elastic-scattering observables.

From Fig. 5 it is clear that the coupling generates quite strong attraction for $r < 3$ fm. The real central DPP is quite undulatory further out but, from Table I, $\Delta J_R = 61.07$ MeV fm^3 indicates substantial overall attraction. The coupling also induces considerable absorption in spite of the remarkable emissive feature at the nuclear center. In particular we note the emissive feature around 6 fm. The real and imaginary spin-orbit DPPs are also markedly undulatory, with, as for every other case in Table I, a substantial net reduction in the real spin-orbit DPP.

B. Evidence for dynamical nonlocality

When two states are both coupled to the elastic channel, but not mutually coupled, then the two formal (nonlocal and l-dependent) DPPs generated by each coupling must add to give the total formal DPP. For example, the CC2 and CC3 formal DPPs add to give the formal CC23 DPP. But this "additivity" of DPPs does not apply to the local equivalents, as calculated here by inversion, for example. Thus, the extent to which local DPPs are additive is significant for the question of the generation of dynamical nonlocality by channel coupling, as explained in Sec. V. Figure 6 presents an example: this figure compares pot4 for the CRC case with the sum of the collective DPP and the DPP due to pickup coupling alone. In that figure, the solid lines are the DPP corresponding to pot4, and are just the difference between the solid and dotted lines in Fig. 5. The dashed lines represent the sum of the DPP for case CRC-noInel in which the coupling to the collective states is omitted, and the DPP for case CC23 in which only the collective states are included. The summed DPPs follow the shape of pot4 for the real central potential reasonably well, and also for the two spin-orbit terms. However, there is a major difference in the imaginary central term. The difference in volume integral given in Table I is not large, presumably because the r^2 weighting in the volume integral picks up the greater depth of the pot4 imaginary potential around 4 fm. The difference exhibited in Fig. 6 is evidence for considerable dynamical nonlocality generated by channel coupling.

C. Dynamic polarization potential for neutrons, coupled reaction channel coupling

The differences between the (p,d) and (n,d) Q values, and other factors noted in Sec. II, suggest that the difference

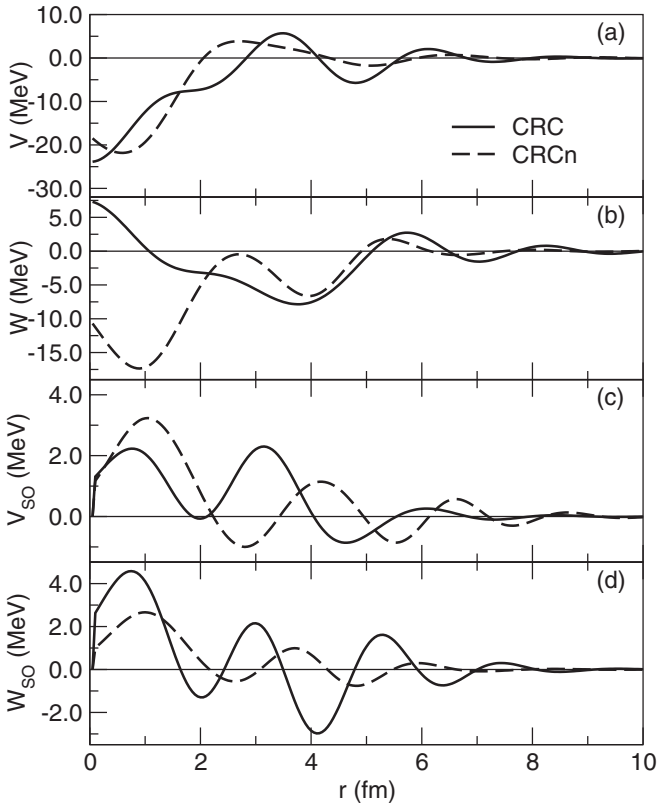

FIG. 7. For 30.1 MeV protons on ^{16}O, inverted potentials for CRC coupling. The dashed lines present the DPP for the CRC case for neutrons. For comparison, the solid lines present the DPP pot4 for protons, as also shown in Fig. 6. Panels (a)–(d) present the real central, imaginary central, real spin-orbit, and imaginary spin-orbit terms, respectively.

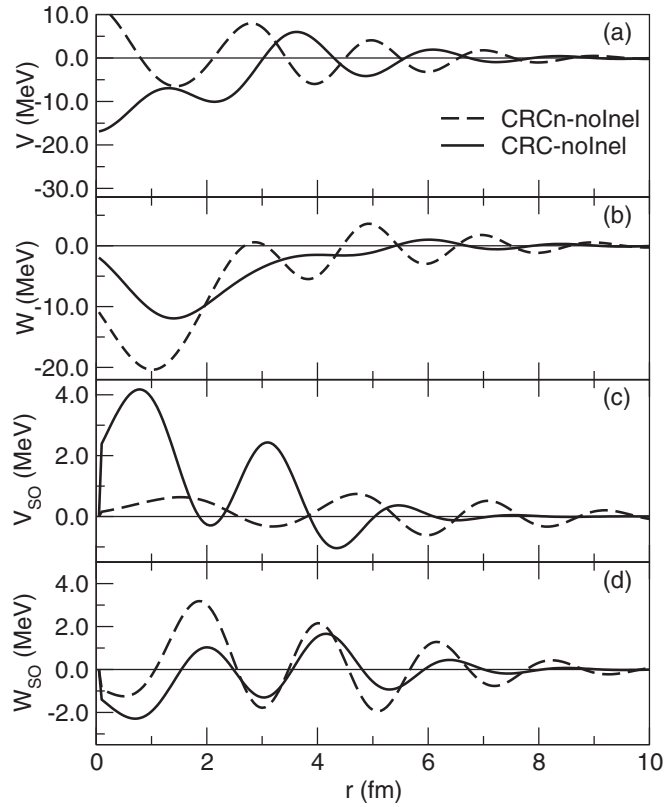

FIG. 8. For 30.1 MeV protons and neutrons on ^{16}O, inverted potentials for CRC coupling without inelastic scattering (cases CRC-noInel and CRCn-noInel). The solid lines present the DPP for protons and the dashed lines present the DPP for neutrons. Panels (a)–(d) present the real central, imaginary central, real spin-orbit, and imaginary spin-orbit terms, respectively.

between the CRC DPPs for neutrons and protons will be greater than for the DPPs due to inelastic scattering alone. From Table I we see that, comparing the CRC-noInel with CRCn-noInel cases, the pickup cross section for the neutron case is greater by a factor of 1.68 than for protons. In contrast, the increase in reaction cross section, ΔCS, induced by (p,d) and (n,d) pickup coupling, is smaller for neutron scattering.

We now consider the CRC and CRCn cases, i.e., including both pickup and inelastic coupling. The dashed lines in Fig. 7 compare the neutron DPP for the CRCn case with that for the proton case. The general tendency for attraction and absorption for a region near $r = 4$ fm is similar for the two cases (inelastic channels are included in both), but otherwise it is the differences that are most apparent. In particular, for neutrons there is strong absorption for $r < 2$ fm, in contrast to the emissiveness in the imaginary part for $r < 1$ fm for protons. These differences are reflected in the volume integrals in Table I; note the negative value of $\Delta J_{\rm SOI}$ in every case of neutron scattering. The differences between the proton and neutron DPPs due to pickup are not surprising in view of the different Q value, bound nucleon form factor, and momentum-matching characteristics. The present results imply that the differences between potentials that *precisely* fit proton and neutron elastic scattering will require more than small adjustments to the Woods–Saxon parameters.

D. Comparison of proton and neutron cases without inelastic scattering

As seen in Sec. III B the differences between the proton and neutron DPPs resulting from coupling to vibrational states are small. However, the effect of the different (p,d) and (n,d) Q values is most directly seen in a comparison of the DPPs for the cases CRC-noInel and CRCn-noInel. From Fig. 8 it is clear that, for this target and energy, pickup of a proton generates a DPP that is quite different from that resulting from pickup of a neutron. The most notable difference is the substantial reduction in the attraction in the real central part for $r < 3$ fm. The undulations for $r > 3$ fm appear to be displaced inward compared with those resulting from the pickup of a neutron in the proton OMP. The effect for $r < 3$ fm corresponds to the reduction of $\Delta J_{\rm R}$ from 39.30 MeV fm^3 for (p,d) coupling to 7.70 MeV fm^3 for (n,d) coupling; see Table I. For the central imaginary term, the (n,d) coupling appears to result in markedly greater undulations, but the overall difference in $\Delta J_{\rm I}$ is small.

E. Dependence on optical model potential parameters

Even with Woods–Saxon-like potentials, the total number of parameters in the nucleon and deuteron channels of coupled

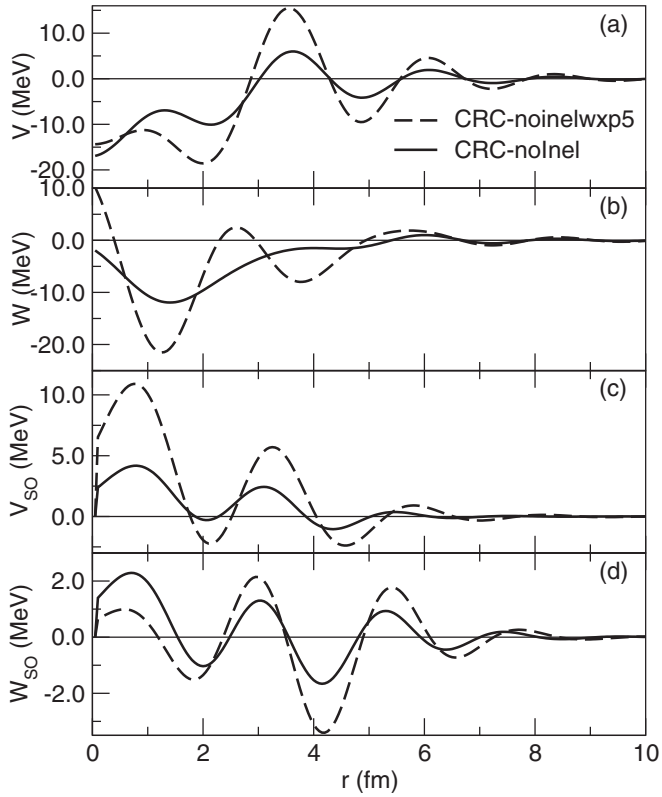

FIG. 9. For 30.1 MeV protons on ^{16}O, inverted potentials for CRC coupling without inelastic scattering (cases CRC-noInel and CRC-noInelwxp5). The solid lines present the DPP for protons for case CRC-noInel and the dashed lines present the DPP for protons when the imaginary part of the deuteron OMP is halved, CRC-noinelwxp5. Panels (a)–(d) present the real central, imaginary central, real spin-orbit, and imaginary spin-orbit terms, respectively.

reaction channel calculations is large. Optimizing all parameters for all observables, for each choice of channel couplings, is a formidable task that we have not attempted. However, it is a relatively simple matter to test, right through to the inversion and determination of DPPs, the effect of changing particular single parameters. As a single example, we do this for the imaginary part of the deuteron OMP in the CRC-noInel case. Halving the depth of the imaginary deuteron potential leads to the results shown in the CRC-noinelwxp5 line of Table I. We find that the reduced absorption increases $\Delta J_{\rm I}$ and ΔCS and reduces $\Delta J_{\rm R}$. One reason for choosing to change the deuteron absorption is the observation that the empirical deuteron OMP includes the effect of the coupling to stripping channels, an effect that is implicit in the CRC calculations. There is also the possibility that absorption from the deuteron channel might be a "doorway" for absorption from the strongly coupled proton channel via the deuteron absorptive potential. However, the fact that the reduced absorption increases $\Delta J_{\rm I}$ and ΔCS suggests otherwise. Decreasing the deuteron absorption markedly increases the effect of coupling on the spin-orbit components. A comparison of the CRC-noInel and CRC-noinelwxp5 DPPs in Fig. 9 reveals the effect on the radial form of the DPPs. For the real central DPP, the overall shape is the same but the amplitude of the undularity is increased. The same is true for the other terms apart from the appearance of emissivity near 2.5 fm in the imaginary central term. It is therefore likely that an increase in the absorptive term in the imaginary part would lead to a lessening of the undularity of the DPPs, and this might be worth pursuing in future work.

Modifying particular parameters can, in principle, offer a means toward understanding reaction dynamics; this is one example of the many tests that are possible within the coupled-channel-plus-inversion framework. Reference [4] presents an extensive study of the effect of changes of OMP parameters for the case of (p,d) coupling on ^{40}Ca.

V. DYNAMICAL NONLOCALITY

There has been considerable interest recently in the consequences for nuclear reaction calculations of the nonlocality that can be attributed to exchange processes; for exchange effects in deuteron reactions see Ref. [33] and reference therein. Less attention has been paid to the nonlocality arising from reaction processes, as formulated, for example, by Feshbach [9,10]; see also Refs. [8,12]. As noted above and discussed in Ref. [13] and elaborated in Ref. [18], the formal nonlocal DPPs arising from particular coupled channels that are included together but that are not mutually coupled must add to give the sum of the nonlocal contribution from those coupled channels separately. However, this additivity does not apply to the local and l-independent equivalents of the nonlocal DPPs which will not add closely. A simple argument why the local equivalents of nonlocal potentials do not add is given in Ref. [13].

The present calculations provide evidence for the dynamical nonlocality of the DPPs due to coupling. This refers to the formal DPPs, the local equivalents of which we have determined by inversion of the elastic scattering S matrix. Evidence in the form of the DPPs in the CRC case was given in Sec. IV B, but further evidence can be found in Table I where the lines labeled CC2+CC3, CRC-noInel+CC23, and CRCn-noinel+CC23n present volume integrals and other quantities that can be compared with, respectively, the lines labeled CC23, CRC, and CRCn. We find that the CC2 and CC3 values of $\Delta J_{\rm I}$ add very closely to the CC23 value but all other quantities add less precisely. Figure 3 shows that, on a point-by-point basis, all components add very closely for r away from the nuclear center. As well as being consistent with the interpretation of dynamical nonlocality, this also argues against any suggestion that the undularity is an artifact of the inversion. By contrast, the value of ΔCS for CC23 is less than the sum of the values for CC2 and CC3. This seems very natural since one coupling (to either 2^+ or 3^-) will remove less flux when the other process is also removing flux. The nonadditivity of the ΔCS values is not, however, evidence for dynamical nonlocality.

The situation is different when reaction channel coupling is involved. The $\Delta J_{\rm I}$ values for CC23 and CRC-no-Inel do not add to the value for CRC: 122.26 is not that close to 134.56. On the other hand the ΔCS value for CRC-noIn+CC23 greatly exceeds the value for CRC (286.44 cf. 229.49). In short, ΔCS and $\Delta J_{\rm I}$ behave very differently.

We conclude that pickup coupling induces a dynamically nonlocal DPP. However, the formal DPP [8,9,12] is l dependent as well as nonlocal, and it is the l dependence that results in

the undularity of the local DPPs that we have presented; see Ref. [17].

The calculations presented here show that it is easy to explore the effect of changing particular parameters by using the coupled channel plus inversion technique, but giving a convincing physical explanation of the results is not always easy.

VI. DISCUSSION OF UNDULARITY AND INVERSION UNCERTAINTY

Various markedly wavy potentials have been presented that exhibit features that are not found in standard phenomenological potentials. It is reasonable to ask two questions: (i) do channel couplings such as we have introduced really imply wavy shapes in the nucleon OMP, and (ii) why are wavy shapes not commonly found when fitting elastic-scattering data?

We first briefly answer the second question by pointing out that published fits to (the actually quite rare) precise and complete data seldom achieve close to $\chi^2/F \sim 1$; for further discussion, see Ref. [1]. We can cite one case [34] where model-independent fitting was apparently terminated when fits were imperfect and just when undularity might have appeared.

Concerning the first question, we first point to the extensive success that has been achieved in a wide range of cases applying the same coupled channel and coupled reaction channel formalism (with full nonorthogonality correction, finite range coupling, etc.) that has been employed here. The key question, therefore, is the uniqueness of the potentials found by inversion. The uniqueness of inverted potentials is actually a deep formal problem, but a pragmatic approach exploiting the character of the IP method has been applied successfully in a wide range of cases; see Refs. [27–29].

One aspect of the possible ambiguity problem was illustrated in Sec. IV A, especially Fig. 5, where it was shown that reducing the inversion σ by means of further iterations improved the fit to S_{lj} just for high partial waves. The high partial waves in question, which lead to increased undularity, make an extremely small contribution to those observables that are currently measured. We have chosen in this work to present in Table I and the figures the characteristics of inverted potentials that give complete fits to S_{lj} for all values of l for which it was calculated. It is interesting to speculate whether measurement of Wolfenstein's spin-rotation parameter [35] might discriminate between solutions. From Fig. 5 it can be seen that pushing the iteration to lower σ makes very little difference to the components of the potential that are larger in magnitude.

A pragmatic approach to evaluating ambiguities in the inverted potentials is the application of alternative inversion bases [28,29]. The inversion basis leading to the potentials characterized in Table I and shown in the corresponding figures employed Gaussian functions. Here we present results for the CRC case in which a Bessel function inversion basis was applied. The resulting potential was characterized by the quantities presented in Table II which may be compared with the same quantities in the CRC line of Table I. The CRC potentials inverted with Gaussian and Bessel function bases are compared in Fig. 10, which also includes the bare potential.

TABLE II. Characteristics of inverted potentials using Bessel-function inversion bases. rms radii in fm, volume integrals in MeV fm^3.

Case	ΔJ_R	ΔJ_I	ΔJ_{SOR}	ΔJ_{SOI}	ΔCS
CC2	2.58	16.44	−2.061	2.037	31.22
CRC (pot4)	58.34	138.2	−13.04	5.533	222.49

The more general question is why do undulations occur? The best clue comes from model calculations in which smooth (e.g., Woods–Saxon) l-independent potentials are modified by an overall factor just for partial waves with l less than some value L for which $|S_L|$ is about 0.5; see, for example, Refs. [16,17]. The key point is that S_l generated by a smooth potential for which the overall strength changes with l, over a narrow range of l, simply cannot be represented by a smooth l-independent potential. We conclude from this that the channel coupling effects evidently have different proportional effects on the potential for high l and low l. If the effect for low l is, for example, repulsive, this results in a potential that cannot be smoothly matched across radii corresponding to the l-transition region without "overshoots" leading to undulations. From this

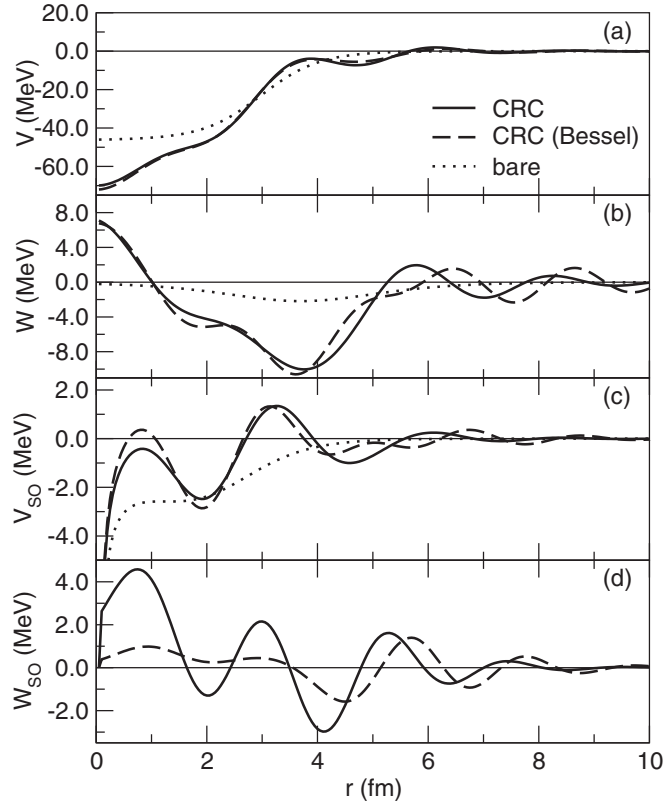

FIG. 10. For 30.1 MeV protons on ^{16}O, comparing inverted potentials for the CRC case for alternative inversion bases. The dotted lines give the four components of the bare potential: Panels (a)–(d) present the real central, imaginary central, real spin-orbit, and imaginary spin-orbit terms, respectively. The solid lines present the inverted potential obtained using IP inversion with a Gaussian function basis; the dashed lines present the result of IP inversion using a Bessel-function basis.

perspective, it seems remarkable that the l-independent OMP is so successful ... if fits to data are not examined closely.

VII. SUMMARY AND GENERAL CONCLUSIONS

The initial aim of this research was to demonstrate that it is not unphysical for the nuclear OMP to have undulations and even have imaginary parts with emissive radial regions. Such undulations are a property [17] of the l-independent potentials that are S-matrix equivalent to l-dependent potentials that have been found to fit closely precise differential cross-section and analyzing-power data over a wide angular range. The present work demonstrates that standard reaction theory does indeed predict an undulatory contribution to the OMP, including emissive regions. The radial shapes of the DPPs that arise from channel coupling show that the uniform renormalization of folding model potentials is not a satisfactory way of correcting such potentials for channel coupling effects.

There are some obvious related questions: (Q1) Why do smooth potentials appear to work so well? (Q2) Does the nucleon-nucleus interaction really have peaks and valleys and if not, why not? There is also a meta-question: (MQ) There have been previous indications of wavy potentials, so why is the possibility generally ignored?

We do not attempt to answer the last question here, but things can be said about the first two. The answer to Q1 is that smooth potentials seldom do as well as wishful thinking suggests. Optical model fitting usually stops when χ^2/F is much greater than one; this is effectively an unacknowledged commitment to undularity-free potentials. For more on this subject, see Ref. [1]. Regarding Q2: for there not to be undularity, including emissive regions, the reaction formalism would have to be demonstrably wrong, or there would have to be many neglected contributions leading to some sort of smoothing-out effect. That is where the ^{16}O case is of interest since, with this light nucleus, there is less scope for a complete averaging-out effect. It would indeed be of interest to pursue progressively more complete calculations, with attention given to the double counting problem. If optimal nucleon OMPs that fit precise and complete datasets have no undularity, the question is, why not?

In the course of this research many interesting phenomena have been found that we have not explained: for example, why does coupling to the 3^- state reduce absorption from all other processes whereas coupling to the 2^+ state increases absorption from all other processes? Answers to such questions await a comprehensive understanding of direct reactions with protons. We have begun similar calculations for protons and neutrons on ^{40}Ca.

A general comment: virtually all proton studies of elastic scattering are incomplete, lacking measurements of the Wolfenstein spin-rotation parameter R [35]. For the significance of R, see Refs. [36,37]. But even worse is the extreme sparseness of analyzing-power data for neutron elastic scattering. This makes an experimental evaluation of the neutron-proton difference suggested by the present work effectively impossible at the present time. Although an understanding of the neutron-nucleus interaction is important for, among other things, the astrophysical r process, this understanding remains incomplete.

[1] R. S. Mackintosh, Eur. Phys. J. A **53**, 66 (2017).
[2] J. M. Cameron, J. R. Richardson, W. T. H. van Oers, and J. W. Verba, Phys. Rev. **167**, 908 (1968).
[3] H. B. Eldridge, S. N. Bunker, J. M. Cameron, J. R. Richardson, and W. T. H. van Oers, Phys. Rev. **167**, 915 (1968).
[4] R. S. Mackintosh and N. Keeley, Phys. Rev. C **85**, 064603 (2012).
[5] R. S. Mackintosh and N. Keeley, Phys. Rev. C **90**, 044601 (2014).
[6] A. M. Kobos and R. S. Mackintosh, J. Phys. G: Nucl. Phys. **5**, 97 (1979).
[7] R. S. Mackintosh, arXiv:1302.1097v5.
[8] G. R. Satchler, *Direct Nuclear Reactions* (Clarendon Press, Oxford, 1983).
[9] H. Feshbach, Ann. Phys. (NY) **5**, 357 (1958).
[10] H. Feshbach, Ann. Phys. (NY) **19**, 287 (1962).
[11] F. G. Perey, Phys. Rev. **131**, 745 (1963).
[12] G. H. Rawitscher, Nucl. Phys. A **475**, 519 (1987).
[13] R. S. Mackintosh and N. Keeley, Phys. Rev. C **81**, 034612 (2010).
[14] N. Keeley and R. S. Mackintosh, Phys. Rev. C **90**, 044602 (2014).
[15] R. S. Mackintosh, Y. Hirabayashi, and S. Ohkubo, Phys. Rev. C **91**, 024616 (2015).
[16] R. S. Mackintosh, Phys. Rev. C **94**, 034602 (2016).
[17] R. S. Mackintosh, arXiv:1705.07003.
[18] R. S. Mackintosh and N. Keeley, arXiv:1610.07378.
[19] I. J. Thompson, Comput. Phys. Rep. **7**, 167 (1988).
[20] T. Kibédi and R. H. Spear, At. Data Nucl. Data Tables **80**, 35 (2002).
[21] E. Strano, D. Torresi, M. Mazzocco, N. Keeley, A. Boiano, C. Boiano, P. Di Meo, A. Guglielmetti, M. La Commara, P. Molini, C. Manea, C. Parascandolo, D. Pierroutsakou, C. Signorini, F. Soramel, D. Filipescu, A. Gheorghe, T. Glodariu, J. Grebosz, S. Jeong, Y. H. Kim, J. A. Lay, H. Miyatake, M. Nicoletto, A. Pakou, K. Rusek, O. Sgouros, V. Soukeras, L. Stroe, N. Toniolo, A. Vitturi, Y. Watanabe, and K. Zerva, Phys. Rev. C **94**, 024622 (2016).
[22] M. Pignanelli, H. V. von Geramb, and R. De Leo, Phys. Rev. C **24**, 369 (1981).
[23] C. M. Perey and F. G. Perey, At. Data Nucl. Data Tables **17**, 1 (1976).
[24] R. V. Reid, Jr., Ann. Phys. (NY) **50**, 411 (1968).
[25] F. Flavigny, A. Gillibert, L. Nalpas, A. Obertelli, N. Keeley, C. Barbieri, D. Beaumel, S. Boissinot, G. Burgunder, A. Cipollone, A. Corsi, J. Gibelin, S. Giron, J. Guillot, F. Hammache, V. Lapoux, A. Matta, E. C. Pollacco, R. Raabe, M. Rejmund, N. de Séreville, A. Shrivastava, A. Signoracci, and Y. Utsuno, Phys. Rev. Lett. **110**, 122503 (2013).
[26] R. S. Mackintosh and A. M. Kobos, Phys. Lett. B **116**, 95 (1982).
[27] S. G. Cooper and R. S. Mackintosh, Inverse Probl. **5**, 707 (1989).
[28] V. I. Kukulin and R. S. Mackintosh, J. Phys. G **30**, R1 (2004).
[29] R. S. Mackintosh, Scholarpedia **7**, 12032 (2012).

[30] S. G. Cooper, *Notes for Imago Users*, Open University report (1999), unpublished, available upon request.
[31] S. G. Cooper and R. S. Mackintosh, Phys. Rev. C **54**, 3133 (1996).
[32] S. G. Cooper, Nucl. Phys. A **618**, 87 (1997).
[33] L. J. Titus, F. M. Nunes, and G. Potel, Phys. Rev. C **93**, 014604 (2016).
[34] R. Alarcon, J. Rapaport, and R. W. Finlay, Nucl. Phys. A **462**, 413 (1987).
[35] L. Wolfenstein, Annu. Rev. Nucl. Sci. **6**, 43 (1956).
[36] A. M. Kobos, R. S. Mackintosh, and J. R. Rook, Nucl. Phys. A **389**, 205 (1982).
[37] R. S. Mackintosh and A. M. Kobos, unpublished, scanned copy available (1980).